Ann. Geophys., 26, 2253–2263, 2008
www.ann-geophys.net/26/2253/2008/

Annales Geophysicae

Bistatic observations of large and small scale ULF waves in SPEAR-induced HF coherent backscatter

T. K. Yeoman[1], **L. J. Baddeley**[2], **R. S. Dhillon**[1], **T. R. Robinson**[1], **and D. M. Wright**[1]

[1]Dept. of Physics and Astronomy, University of Leicester, University Road, Leicester, LE1 7RH, UK
[2]EISCAT Scientific Association, 98123 Kiruna, Sweden

Received: 8 January 2008 – Revised: 15 April 2008 – Accepted: 24 April 2008 – Published: 5 August 2008

Abstract. HF radar backscatter which has been artificially-induced by a high power RF facility has been demonstrated to provide ionospheric electric field data of unprecedented temporal resolution and accuracy. Here such data, induced by the SPEAR high power radar on Svalbard, are used to investigate ULF wave processes observed by the CUTLASS HF radars. Observations are presented of both waves with a large-scale nature, driven externally to the magnetosphere and those with small azimuthal scale lengths, driven by wave-particle interactions. For ULF wave events with large azimuthal scale lengths an excellent agreement in the observed wave polarisation ellipse is found between the radar observations and ground-based magnetometer data. In contrast, for the small scale events, no ground-based magnetic counterpart is observed. Indeed the data from the two CUTLASS radars seem inconsistent, and each radar must be interpreted separately, as the spatial resolution of the radars is sufficient to resolve the wave characteristics along the radar beams, but insufficient to resolve the wave characteristics across the beams. A high azimuthal wave number (m) wave with a period of 300 s and $m\sim-60$ is observed to occur over Svalbard at ∼14:00 magnetic local time. This confirms the existence of waves driven by wave-particle interactions with trapped particle populations in the outer magnetosphere. A comparison of the observed wave characteristics with previous, lower latitude, observations suggests that these high latitude waves have a similar azimuthal scale size to those generated in the inner magnetosphere; the azimuthal wave number of -60 observed in the present study is comparable to previous values of -20–-50, but suggests an increase of m with latitude. A similar energy source in drifting proton populations is also suggested, but with lower characteristic proton energies of 10 keV implicated at high latitude, compared to the 20–60 keV energies invoked for previous lower latitude observations.

Correspondence to: T. K. Yeoman
(tim.yeoman@ion.le.ac.uk)

Keywords. Ionosphere (Active experiments) – Magnetospheric physics (MHD waves and instabilities) – Space plasma physics (Wave-particle interactions)

1 Introduction

Magnetospheric Ultra Low Frequency (ULF) waves which have an energy source external to the Earth, such as an impulse in the solar wind, solar wind buffeting, or the Kelvin-Helmholtz instability on the magnetopause are, in general, characterised by small effective azimuthal wavenumbers, m, (or equivalently a large scale size in the azimuthal direction). In contrast ULF waves with small azimuthal scale lengths, high-m ULF waves (generally waves with $m>15$), have their energy source in drifting energetic particle fluxes, through drift and drift-bounce resonance interactions. Such high-m waves are presently a topic of considerable importance in both theoretical and experimental studies. Energetic particles entering the Earth's inner magnetosphere from the magnetotail will experience gradient-curvature drift and thus move around the Earth, constituting part of the global ring current. Such drifting particles can drive MHD wave modes through wave-particle interactions, leading to perturbations in the electric and magnetic fields in the magnetosphere and ionosphere when free energy is available to the wave. It has been suggested (e.g. Southwood, 1976; Hughes et al., 1979) that the part of the ion distribution function which is able to feed energy into the wave is that where $\partial f/\partial W>0$ where f is the ion distribution function and W is the energy. Such non-Maxwellian ion distribution functions, often termed "bump-on-tail" distributions, can be created quite commonly by naturally-occurring processes in the magnetosphere, such as substorm-associated particle injections or other particle acceleration processes. Subsequent to such an injection the ions are subject to gradient-curvature and $\mathbf{E}\wedge\mathbf{B}$ drifts and move westwards, arriving at a given magnetic

Published by Copernicus Publications on behalf of the European Geosciences Union.

local time at different universal times due to the energy dependence of magnetospheric drift paths. Even under steady state conditions particles follow energy-dependent drift paths which can lead to the formation of such bump-on-tail distributions (Cowley and Ashour-Abdallah, 1976; Ozeke and Mann, 2001). Subsequent to such an injection and drift process, on occasion particles will match the local drift-bounce resonance condition (Southwood et al., 1969),

$$\omega_{\text{wave}} - m_{\text{wave}}\omega_{\text{drift}} = N\omega_{\text{bounce}}, \quad (1)$$

where N is either zero (drift resonance) or an integer (usually ± 1, drift bounce resonance). In either case ω_{wave}, ω_{bounce}, and ω_{drift} are the angular frequencies of the wave, the proton bounce, and the proton azimuthal drift, respectively. Such wave-particle interactions are processes of fundamental importance in collisionless astrophysical plasmas.

The ionosphere modifies the magnetospheric ULF wave signature, leading to rotation and attenuation of the wave magnetic signature detected on the ground (e.g. Hughes and Southwood, 1976; Hughes, 1983). This attenuation of the pulsation magnetic perturbation below the ionosphere is proportional to e^{-kz} (e.g. Hughes and Southwood, 1976) where k is the field perpendicular component of the wave number and z is the E-region height. It is thus clear that ground magnetometer data is far from optimal for the study of high-m ULF waves, and that direct observation in the ionosphere or magnetosphere is usually required. In previous work, two categories of particle-driven waves have been particularly intensively studied with ground-based data: storm time pulsations and giant "Pg" waves, which are dusk and dawn sector phenomena, respectively.

Storm time Pc5 pulsations have been seen in STARE (the Scandinavian Twin Auroral Radar Experiment; Greenwald et al., 1978) data (Allan et al., 1982, 1983). This instrument had a spatial resolution of $\sim$20 km and a temporal resolution of 20 s. Storm time Pc5 pulsations are compressional waves of high m number (m=$-$20–$-$80; here negative m is taken to represent westward phase propagation) and frequency in the Pc5 range (1.7–6.7 mHz) which are associated with a drift resonance source mechanism. Drift resonance involves fundamental wave modes, with the electric field symmetric about the equator (i.e. an equatorial electric field antinode). Storm-time Pc5s are observed in the dusk sector during magnetically disturbed intervals. Similar waves, but with an equatorward phase motion, have been seen in SABRE (the Sweden And Britain auroral Radar Experiment; Nielsen et al., 1983) and BARS (Bistatic Auroral Radar System; McNamara et al., 1983) coherent radar systems in the dusk sector by Yeoman et al. (1992) and Grant et al. (1992), respectively. Again a spatial resolution of $\sim$20 km and a temporal resolution of 20–30 s was available from these instruments. These previous observations of equatorward propagating waves are the most similar observations to those which will be presented here.

The second class of particle driven ULF waves of interest are giant "Pg" pulsations which have been observed on the ground as well as by orbiting satellites at times when geomagnetic conditions are quiet. Pgs are an example of a particle-driven ULF wave which may be studied with ground-based magnetometers. Chisham and Orr (1991) presented a statistical study of 34 of these events observed on the EISCAT magnetometer cross network in northern Scandinavia. They found a peak in occurrence of these waves in the dawn/prenoon sector and no events were observed in the afternoon. The average value of the azimuthal wave number was -26 for the 34 events. Pgs have been related to drift-bounce resonance mechanisms with both symmetric (e.g. Takahashi et al., 1992) and antisymmetric (e.g. Chisham and Orr, 1991) wave modes, and the wave-particle interaction responsible for their generation thus remains controversial.

Recent results from DOPE (the DOppler Pulsation Experiment; Wright et al., 1997) at Tromsø, northern Norway (a system with a spatial resolution of $\sim$5 km and a temporal resolution of $\sim$12 s) have demonstrated the existence of populations of high-m waves in both the morning and afternoon sectors (Yeoman et al., 2000). In this case the morning sector waves were the most populous, and had m-numbers of order 100, high enough to screen the waves completely from ground magnetometers. The structure and occurrence of such particle-driven waves have been studied by a number of authors in the magnetosphere with in situ spacecraft data, for both case studies (e.g. Hughes et al., 1979; Takahashi et al., 1990) and statistically (e.g. Kokubun, 1985; Takahashi et al., 1985; Anderson et al., 1990; Woch et al., 1990; Engebretson et al., 1992; Lessard et al., 1999). These studies are largely consistent with the ground-based results, identifying a strong population of particle-driven waves in the dusk sector. Events are also detected near dawn, however, and a variety of wave-particle interaction modes have been invoked. Yeoman and Wright (2001) presented ULF wave observations close to local noon using the HF radar artificial backscatter technique at Tromsø which demonstrated both wave activity characteristic of drift-bounce resonance and wave activity characteristic of drift resonance activity, with the latter waves showing equatorward phase propagation. Previous studies, therefore, have established the importance of ULF waves driven by wave-particle interactions in the inner magnetosphere. What remains unclear is the importance of these processes at higher latitudes, where the geomagnetic field lines are often open, and the trapping of energetic particles is more difficult. In this paper, the HF radar artificial backscatter technique is used at the Space Plasma Exploration by Active Radar (SPEAR, Wright et al., 2000; Robinson et al., 2006) system on Svalbard in order to provide a new dataset for the study of such particle-driven ULF waves at very high latitudes.

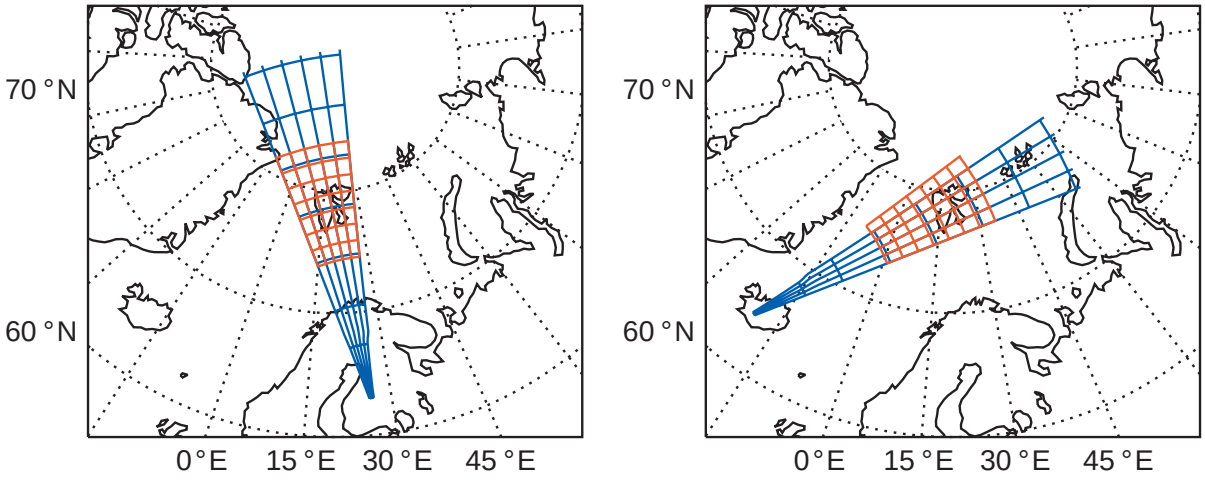

Fig. 1. The fields of view of Channel A (red) and Channel B (blue) of the Hankasalmi, Finland and Þykkvibær, Iceland SuperDARN radars during artificial backscatter experiments with the SPEAR system

2 Instrumentation

The data presented here result from the generation of HF coherent backscatter from artificial ionospheric irregularities in the fields-of-view of the SuperDARN radars at Hankasalmi and Þykkvibær with SPEAR (Wright et al., 2000; Robinson et al., 2006), the new ionospheric modification facility on Svalbard. Details of SuperDARN are given in Greenwald et al. (1995) and Chisham et al. (2007). Figure 1 presents the beam and range locations for the 15 km range gate radar scan modes used in this study. For the SPEAR experiments, a restricted scan ran on both channels of the radar, one using 45 km range gates, starting at a range of 180 km and the other 15 km range gates, starting at 1485 km. A frequency sweep mode was employed, ranging from 9.9–13.3 MHz, using integration times of 1 or 2 s per beam. Here data for Þykkvibær beam 6 and Hankasalmi beam 9, which intersect over SPEAR, are presented. Previous experiments performed with the EISCAT Tromsø heating facility (Rietveld et al., 1993) have employed a similar scan pattern. In Fig. 1 range gates are marked every 10th gate. For the SPEAR experiments, the full SPEAR array was used (48×2 kW transmitters), in O-mode polarisation, providing an effective radiated power (ERP) of ∼15 MW, between 4–5 MHz. The heater produces artificial electron density irregularities in the F-region ionosphere, which act as targets for the HF radars. The artificial targets result in very high returned backscatter power in comparison to naturally-occurring irregularities. This allows a short integration time to be run on the radar, providing higher time resolution than is normally available.

Data are also presented from the IMAGE (International Monitor for Auroral Geomagnetic Effects; Lühr, 1994) magnetometer station at Longyearbyen (LYR, location 78.20° N, 15.82° E geographic), which has a sampling interval of 10 s.

3 Observations

During the September–October 2006 campaign of SPEAR high power operations two extended intervals of artificial backscatter were observed where simultaneous, collocated data were collected by both the Hankasalmi and Þykkvibær SuperDARN radars. The first of these were observed between 12:00–14:30 UT on 9 October 2006. Figure 2 presents large-scale ULF wave activity during these ionospheric modification experiments. Figure 2a shows colour-coded Hankasalmi beam 9 line-of-sight velocities in the meridional direction as a function of range gate and time. Figure 2b similarly shows colour-coded Þykkvibær beam 6 line-of-sight azimuthal velocities. In each case positive (negative) velocities represent flow towards (away from) the radars. SPEAR started transmitting at 11:00 UT, but ionospheric conditions were not conducive to artificial backscatter generation until 12:25 UT, most probably because the F-region critical frequency, *fo*F2, was below the SPEAR transmit frequency before this time. SPEAR-induced artificial backscatter is apparent in both radar beams after this time, up until 13:50 UT, when it weakens in the Hankasalmi data. Larger velocities are observed in the Þykkvibær radar data, indicating a wave event dominated by the azimuthal velocity component. It is clear that the location of the patch of artificially-generated irregularities varies in time in both radars. This variation is the result of varying HF propagation conditions over the 1-$\frac{1}{2}$hop , ∼2000 km propagation path between the radars and SPEAR, as has been documented by Yeoman et al. (2001). In order to compare appropriate range gates from each radar the centre of the patches of artificial backscatter have been identified, and are marked in Fig. 2a and b with a dashed line. Velocities from these range gates may then be directly compared and combined when strong artificial backscatter

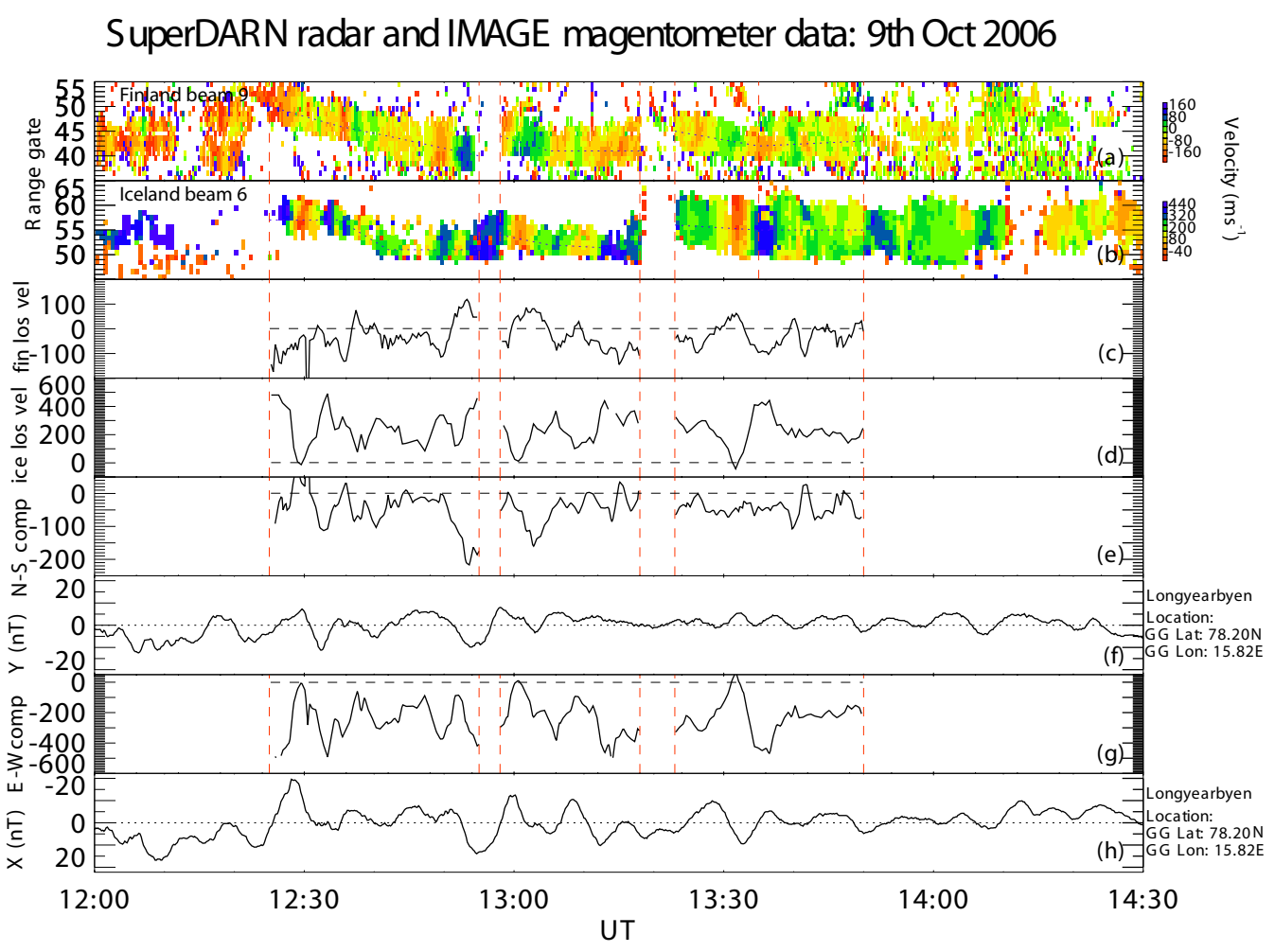

Fig. 2. Large-scale ULF wave activity during the ionospheric modification experiments from 12:00–14:30 UT on 9 October 2006. **(a)** Colour-coded Hankasalmi beam 9 line-of-sight velocities as a function of range gate and time **(b)** Colour-coded Þykkvibær beam 6 line-of-sight velocities as a function of range gate and time **(c)** A timeseries of the line-of-sight velocities taken from the centre of the artificial backscatter shown in panel (a) **(d)** A timeseries of the line-of-sight velocities taken from the centre of the artificial backscatter shown in panel (b) **(e)** The north-south velocity component, resolved from the line-of-sight components displayed in (c) and (d) **(f)** Longyearbyen east-west (Y) component magnetic field **(g)** The east-west velocity component, resolved from the line-of-sight components displayed in (c) and (d) **(h)** Longyearbyen north-south (X) component magnetic field. See text for details.

returns are measured from both radars, and such intervals are presented, delineated by vertical dashed lines in Fig. 2c–e and g. Figure 2c shows a timeseries of the line-of-sight velocities taken from the centre of the artificial backscatter shown in panel (a). Similarly Fig. 2d presents a timeseries of the line-of-sight velocities taken from the centre of the artificial backscatter shown in panel (b). The north-south velocity component, resolved from the line-of-sight components displayed in Fig. 2c and d is given in Fig. 2e. This may be directly compared with the Longyearbyen east-west (Y) component magnetic field in Fig. 2f. Similarly, the east-west velocity component, resolved from the line-of-sight components displayed in Fig. 2c and d is given in Fig. 2g, and may be compared with the Longyearbyen north-south (X) component magnetic field in Fig. 2h. Note that the scale in Fig. 2h has been reversed to facilitate this comparison. A strong level of similarity is observed between the ionospheric flow velocities and the ground magnetometer data, particularly between the east-west flows and the north-south magnetic field, where the oscillation is strongest.

The comparison between the ionospheric flows due to the ULF wavefield and their ground magnetic counterparts can be examined further by examining the polarisation ellipse of the wave in both datasets. Figure 3 panels (ai–gi) present hodograms derived from the north-south and east-west velocities displayed in Fig. 2 panels (e) and (g), whilst Fig. 3

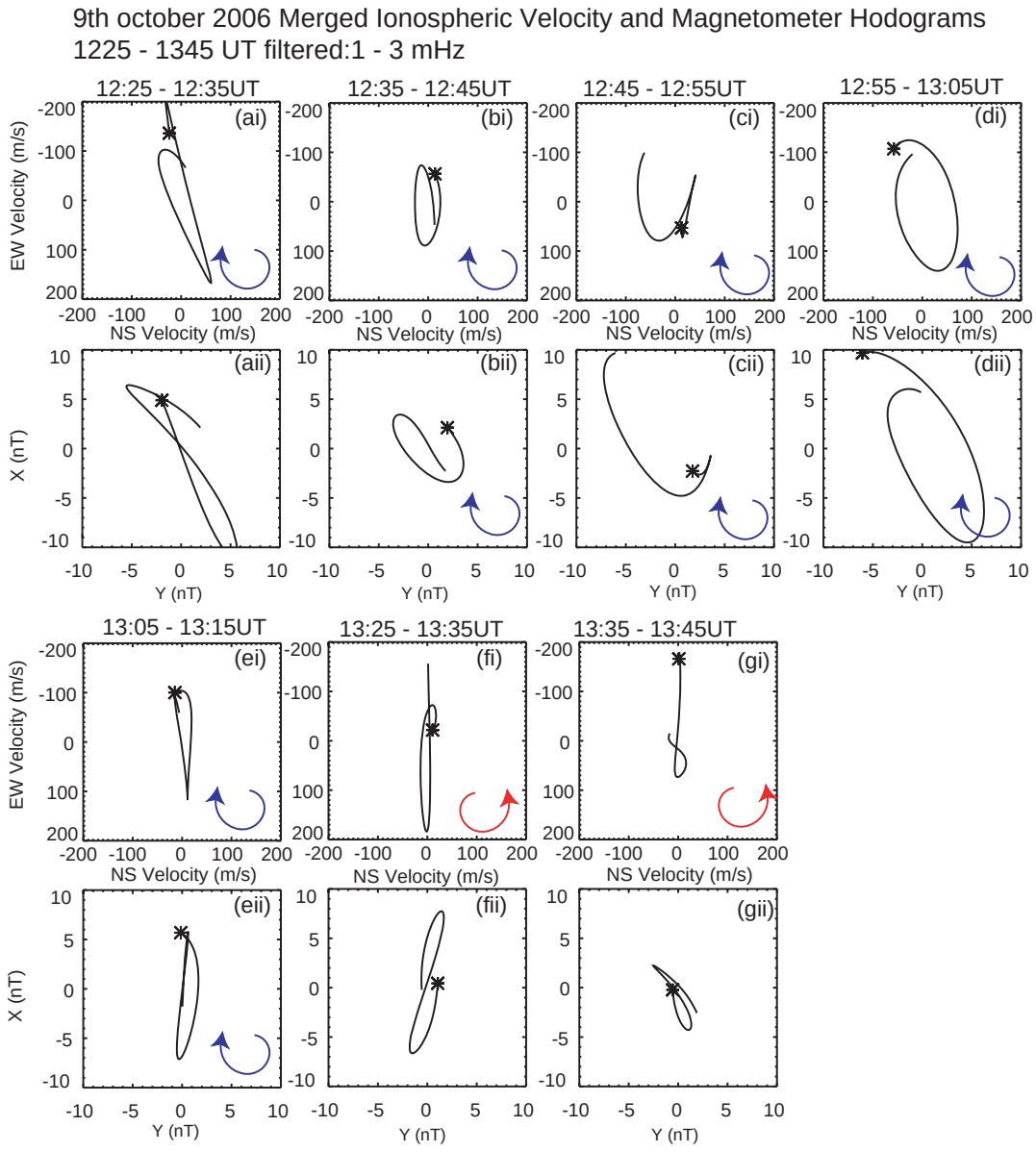

Fig. 3. (ai–gi) Hodograms derived from the north-south and east-west velocities displayed in Fig. 2 panels (e) and (g). **(aii–gii)** Hodograms derived from the east-west and north-south magnetic field displayed in Fig. 2 panels (f) and (h).

panels (aii–gii) present hodograms derived from the east-west and north-south magnetic field displayed in Fig. 2 panels (f) and (h). In each panel there is close agreement between the sense of polarisation, and the ellipticity and orientation of the polarisation ellipse.

A second, and very different interval of ULF wave activity was observed on 12 October 2006, from 11:00–13:00 UT. This interval is presented in Fig. 4. It will be demonstrated that this interval is characterised by small-scale ULF wave activity during the ionospheric modification experiments. Figure 4a shows colour-coded Hankasalmi beam 9 line-of-sight velocities in the meridional direction as a function of range gate and time. Figure 2b similarly shows colour-coded Þykkvibær beam 6 line-of-sight azimuthal velocities, as in Fig. 2 but now as a function of magnetic latitude and time. Magnetic latitude is chosen as in this case a far more consistent radar range location is obtained for the location of the artificial backscatter patches. Figure 4c shows timeseries of the line-of-sight velocities taken from a selection of range gates presented in panel (a), whereas Fig. 4d presents the Longyearbyen east-west (Y) component magnetic field. Similarly Fig. 4e presents a timeseries of the line-of-sight

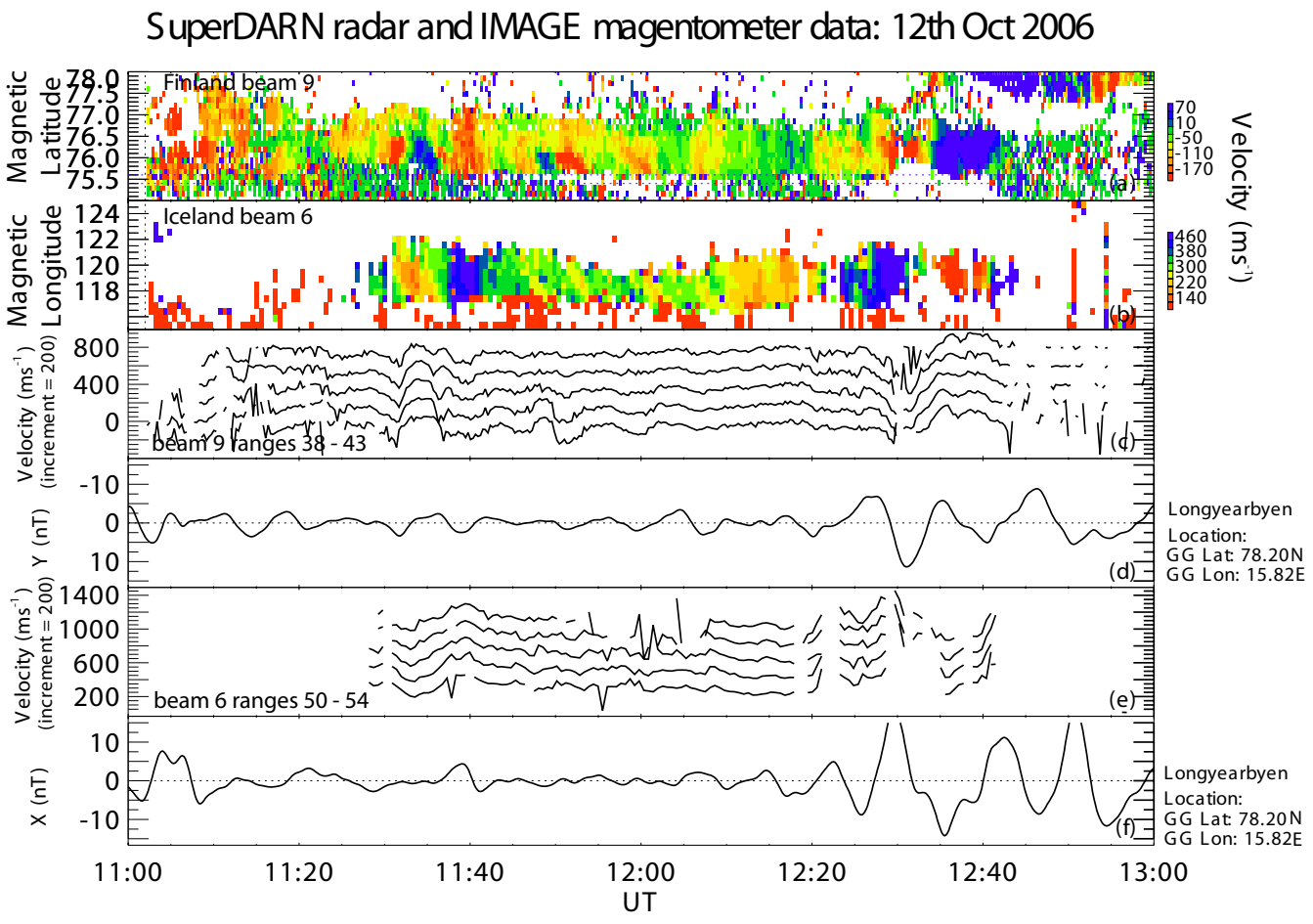

Fig. 4. Small-scale ULF wave activity during the ionospheric modification experiments from 11:00–13:00 UT on 12 October 2006. **(a)** Colour-coded Hankasalmi beam 9 line-of-sight velocities as a function of magnetic latitude and time **(b)** Colour-coded Þykkvibær beam 6 line-of-sight velocities as a function of magnetic latitude and time **(c)** A timeseries of the line-of-sight velocities taken from a selection of range gates presented in panel (a) **(d)** Longyearbyen east-west (Y) component magnetic field **(e)** A timeseries of the line-of-sight velocities taken from a selection of range gates presented in panel (b) **(f)** Longyearbyen north-south (X) component magnetic field.

velocities taken from a selection of range gates presented in panel (b) and Fig. 4f presents Longyearbyen north-south (X) component magnetic field. As with the data presented in Figs. 2 and 3, strong similarities may be seen in the ionospheric velocity data and ground magnetic field data at, for example, ∼11:30 UT and ∼12:20 UT. In this study we will concentrate on an interval of ULF wave activity visible in the line-of-sight data from both radars between 11:40 UT and 12:20 UT. In contrast to the data presented in Figs. 2 and 3, however, this wave activity is not apparent in the ground magnetic field data, and the reasons for this will be investigated next.

In order to investigate this interval of ULF wave activity in more detail, a subset of the colour-coded line-of-sight velocities presented in Fig. 4 is shown in Fig. 5. Figure 5a presents Hankasalmi beam 9 line-of-sight velocities and Fig. 5b Þykkvibær beam 6 line-of-sight velocities. The data from the meridional beam illustrated in Fig. 5a reveals that the wave has rapid equatorward phase propagation, whereas the data from the azimuthal beam illustrated in Fig. 5a reveals rapid westward phase propagation. As described in the introduction, such rapid phase variation effectively shields the variations from the ground magnetic field measurements, such that only direct ionospheric measurements are capable of revealing the wave characteristics. Even in the case of such direct ionospheric measurements, however, the wave characteristics of such small-scale events present a challenge. If data are examined from, for example, adjacent azimuthally-separated beams of the Hankasalmi radar, no convincing evidence is found for the azimuthal phase propagation which is clearly evident from the azimuthally-pointing beams of the Þykkvibær radar as seen in Fig. 5b. This discrepancy is the reason why no direct combination of the data from the two radars was attempted in

Fig. 4, and its explanation requires an examination of the spatial distribution of line-of-sight velocities from both radars.

Such a spatial distribution of line-of-sight velocities, as measured at four representative times during the wave event depicted in Fig. 5, is presented in Fig. 6 in geographic coordinates. The upper row shows data from Hankasalmi and the lower row data from Þykkvibær. The range gates selected for the beams presented in Fig. 5 are here outlined in black for each beam of Hankasalmi and Þykkvibær. Beams 9 (Hankasalmi) and beam 6 (Þykkvibær) presented in Fig. 5 are labelled in Fig. 6. The time intervals presented for the data from each radar in Fig. 6 are marked with vertical dashed lines in the corresponding panels of Fig. 5, and are chosen to encompass a clear phase front of the wave in the radar backscatter, revealing equatorward phase propagation of the region of velocities colour-coded red ($\sim -150\,\mathrm{m\,s^{-1}}$) and westward phase propagation of the region of velocities colour-coded yellow ($\sim +250\,\mathrm{m\,s^{-1}}$) for Hankasalmi and Þykkvibær, respectively. The upper panels of Fig. 6 clearly show the region of velocities colour-coded red migrating downwards, towards lower latitudes. Similarly the lower panels show the region of velocities colour-coded yellow migrating right-to-left, westwards. However, the equatorward migration of the region which is apparent in the upper panels is not apparent in the lower panels, as a result of the geometry of the radar range gates: the 15 km resolution along the beam reveals the wave's structure, whereas the 113 km resolution provided by the radar beam width obscures this phase motion. The converse is true in the lower panels, where the 15 km range resolution is only available in the azimuthal direction. Thus the data from each radar look direction must be treated separately, and not combined as was possible in the analysis of the large scale event depicted in Figs. 2 and 3.

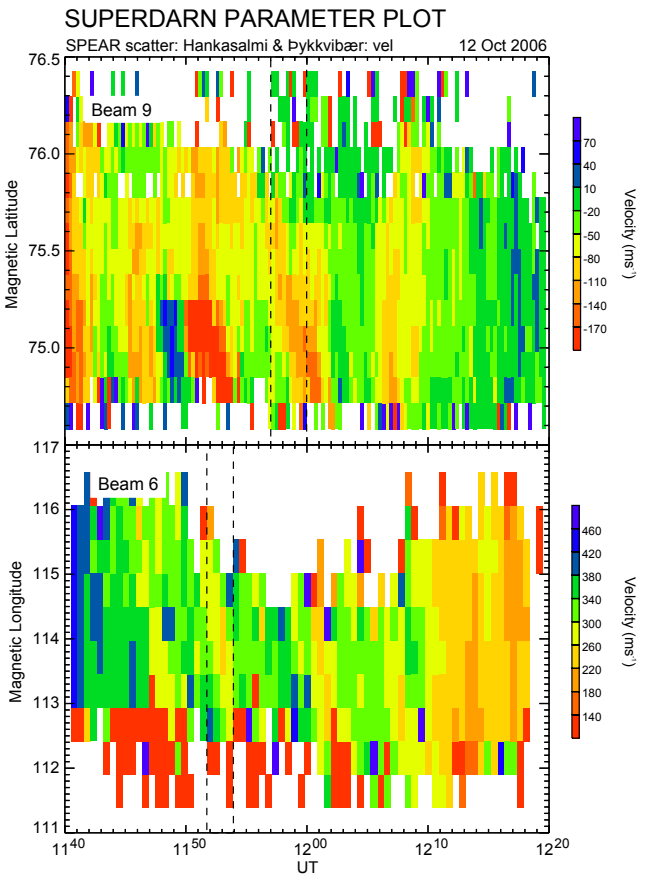

Fig. 5. A detail of the colour-coded line-of-sight velocities presented in Fig. 4 **(a)** Hankasalmi beam 9 line-of-sight velocities **(b)** Þykkvibær beam 6 line-of-sight velocities. A wave with equatorward and westward phase propagation can be observed.

4 Discussion

4.1 Artificial backscatter observations of large-scale ULF waves

Data have been presented from 9 October 2006 illustrating large-scale ULF wave phenomena as measured by backscatter which has been artificially-induced in the Hankasalmi and Þykkvibær SuperDARN radars by the SPEAR high power HF facility on Svalbard. This large-scale ULF wave event displayed a slow evolution of wave phase along the beams from both radars. The line-of-sight components of the radar data were merged into the geographic coordinate system, allowing a direct comparison of ionospheric flows and ground magnetic signatures. A good agreement was observed between the ionospheric flows and the ground magnetic field data, with the wave event being dominant in the east-west ionospheric flows and the north-south magnetic field components. Thus, allowing for the rotation of the ULF wave field as it passed from the magnetosphere, through the ionosphere, to the ground, the polarisation ellipse of the wave as measured by the two techniques was also in excellent agreement, and consistent with that expected for a field line resonance with a toroidal polarisation. The ratio of the ionospheric electric field and ground magnetic field is consistent with previous results using backscatter artificially induced by the EISCAT heater at Tromsø (Yeoman et al., 2006), implying similar ionospheric conductivities and boundary conditions for the ULF wave field at the two widely-separated locations. Thus the utility of artificial backscatter techniques for the investigation of ULF waves and similar dynamics of the convection electric field has been confirmed at these long radar ranges. Such measurements form an important complementary dataset to the data available from the EISCAT Svalbard radar.

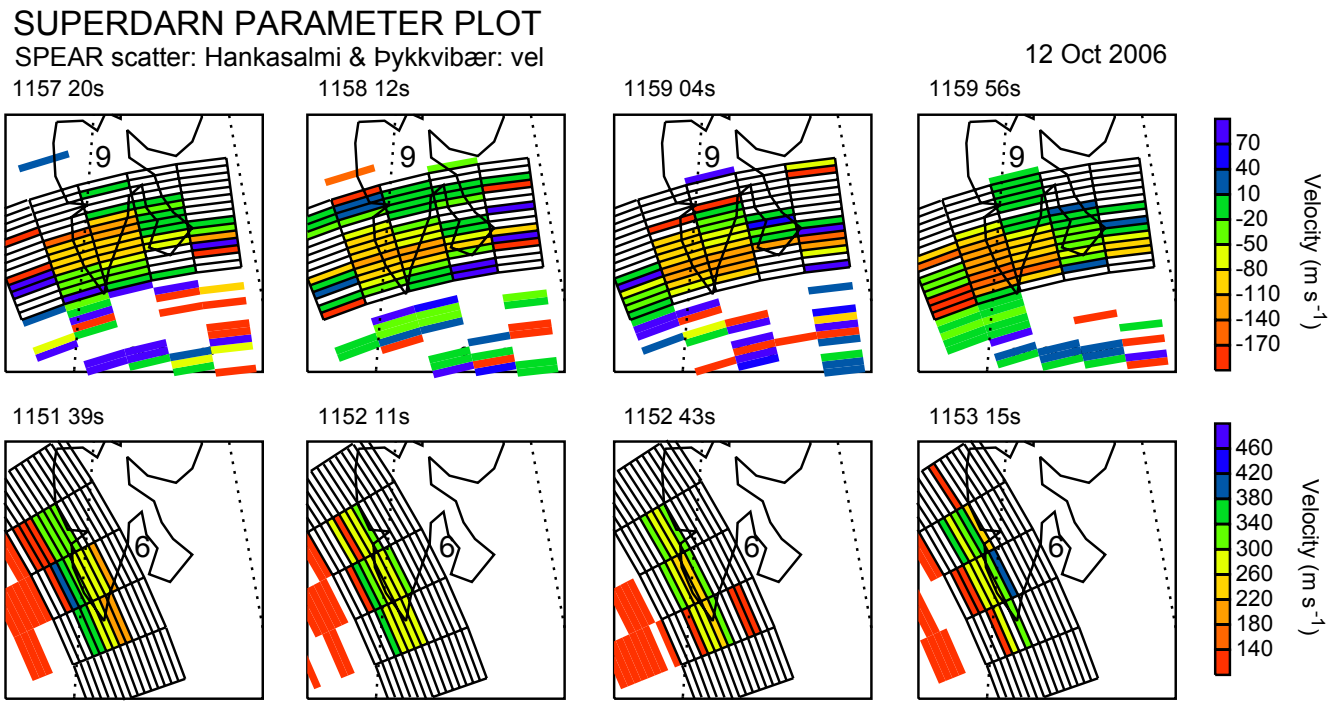

Fig. 6. The spatial distribution of line-of-sight velocities measured at four representative times during the wave event depicted in Fig. 5, in magnetic local time-magnetic latitude coordinates. The upper row shows data from Hankasalmi and the lower row data from Þykkvibær. The range gates selected for the beams presented in Fig. 5 are here outlined in black for each beam of Hankasalmi and Þykkvibær. Beam 9 of Hankasalmi and beam 6 of Þykkvibær, the beams displayed in Fig. 5, are labelled.

4.2 Artificial backscatter observations of small-scale ULF waves

Three days later, on 12 October 2006, a similar artificial backscatter experiment revealed the characteristics of a small-scale ULF wave. In this case the ground magnetic signature of the wave was highly attenuated, rendering the ground magnetometers ineffective in parameterising the wave characteristics. Even the radar backscatter data have to be examined with care in this case, as the spatial resolution of the radar across the beams is insufficient to resolve the phase motion of the wave. Only data from along the radar beams have sufficient resolution to do this, and thus the data from Hankasalmi and Þykkvibær have to be treated separately. Treated thus, following the motion of a wave crest through the fields-of-view of the radars, they reveal an equatorward phase propagation of $\sim$0.4 km s^{-1} and a westward phase propagation of $\sim$0.5 km s^{-1}, equivalent to an azimuthal wave number, m, of ~ -60. This represents the first observations of ULF waves with such characteristics at the high latitudes of Svalbard.

4.3 The origin of the small-scale ULF waves

Whilst the observations of small scale ULF waves presented above represent the first observations of waves of this type at such high latitude, clues as to their generation may be gained from considering previous, lower latitude observations. A number of authors have reported observations of high-m wave events with equatorward phase propagation. Wave events in data from the SABRE (the Sweden And Britain auroral Radar Experiment; Nielsen et al., 1983) radar system at L-shell of $L\sim5$ were first reported by Waldock et al. (1983). These events were further examined by Tian et al. (1991) and Yeoman et al. (1992), and were found to have typical periods of 400 s, with typical m-numbers of ~ -20. These events were interpreted as being the result of a drift resonance process, where N=0 in Eq. (1). The characteristics of the events then implied a wave energy source in a magnetospheric particle population inversion (a bump-on-tail distribution) involving $\sim$60 keV protons. The source of the equatorward phase propagation was attributed by these authors as the plasmapause, as the events were observed primarily at dusk, when the plasmapause is statistically close to L=5. Concurrently, Grant et al. (1992) reported a similar set of observations from the BARS (Bistatic Auroral Radar System; McNamara et al., 1983) radar at $L\sim7.5$. A similar energy source was proposed for these events, but the wave

Table 1. A summary of the characteristics of ULF wave observations showing equatorward phase propagation, and the particle energy of their proposed magnetospheric source.

Study	m	t (s)	L-shell	Implied proton energy (keV)
This study	−60	300	15	10
Grant et al. (1992)	∼−50	∼300	7.5	20
Yeoman and Wright (2001)	−35	260	6.4	50
Yeoman et al. (1992)	∼-20	∼400	5	60

characteristics now implied a proton energy of ∼20 keV. The plasmapause could be ruled out as a significant factor for these observations, as a result of the higher latitude. More recently an equatorward propagating event was observed at intermediate latitudes by Yeoman and Wright (2001), in an experiment which employed an artificial backscatter experiment using the Hankasalmi and Þykkvibær radars in conjunction with the EISCAT heater at Tromsø at L=6.4. Again, drift resonance was implicated as the wave energy source, but now with 50 keV protons. Applying the same reasoning to the event presented in this study, taking the angular drift frequency of the particles to be

$$\omega_{\text{drift}} = \frac{\omega_{\text{wave}}}{m_{\text{wave}}} = \frac{2\pi}{\tau_{\text{wave}} m_{\text{wave}}}, \quad (2)$$

where τ_{wave} is the wave period (i.e. taking N=0 in Eq. 1) yields a proton angular drift frequency of $\sim 3.5 \times 10^{-4}$ rads s^{-1}. Applying the equations for the dependence of proton drift on particle energy as in Yeoman and Wright (2001) then implies an energy source in 10 keV protons at L=15. At these low energies, the drift speed due to gradient-curvature drift and $\mathbf{E} \wedge \mathbf{B}$ drift are comparable, and the radar data in Fig. 4 indicate a variable ionospheric electric field, so there is a significant uncertainty in the value of 10 keV. The characteristics of the ULF wave events with equatorward phase propagation observed by Grant et al. (1992), Yeoman et al. (1992), Yeoman and Wright (2001) and those presented here are summarised in Table 1, along with the energetic particle populations implicated in their generation by the authors concerned. Table 1 shows that whilst wave events are seen with a variety of m-numbers and periods, a clear trend exists in that the energy of the proposed particle population inversion decreases as the L-shell of the observation increases.

In order to verify that the proposed generation mechanism is realistic, it is neccessary to establish whether such populations of energetic particles are likely to exist within the magnetosphere which overlies the ionospheric wave observations. Such a comparison has been performed at the latitudes of Tromsø by Baddeley et al. (2004), who performed a statistical analysis of the local time occurrence of population inversions in the magnetospheric ion distribution functions as measured by the Polar satellite. Subsequently Baddeley et al. (2005b) were able to demonstrate a statistically significant relationship between such population inversions and ionospheric observations of high-m waves. Baddeley et al. (2005a) additionally provided evidence that in the pre-noon sector the drift-bounce resonance mechanism was statistically more likely whereas in the post-noon sector both a drift or drift-bounce resonance interaction was statistically possible. The analysis of magnetospheric ion distribution functions was extended to a wider range of invariant latitudes by Wilson et al. (2006). Figure 7 presents a subset of occurrence distributions of bump-on-tail ion distribution functions taken from Wilson et al. (2006) as a function of particle energy and magnetic local time as observed by the Polar CAMMICE instrument for (a) 60°–67° N magnetic latitude (b) 68°–69° N magnetic latitude (c) 74°–75° N magnetic latitude. In Fig. 7a, at latitudes which correspond to the wave events analysed by Tian et al. (1991), Yeoman et al. (1992) and Yeoman and Wright (2001), it can be seen that whilst the majority of population inversions occur at energies close to 5 keV, some are observed at higher energies close to 50 keV. At higher latitudes, corresponding to the wave events examined by Grant et al. (1992), Fig. 7b reveals that these higher energy population inversions have been lost, but population inversions at energies up to 20 keV remain. At the highest latitudes, corresponding to the event presented here, Fig. 7c reveals that the maximum energy of the population inversion has reduced further, with no events observed above 10 keV. Thus in each case the particle populations inferred in Table 1 represent the highest particle energies at which population inversions are observed to actually occur within the magnetosphere, but Fig. 7 reveals that the implied particle energies can indeed provide the energy source required to explain the observations of equatorward propagating waves over the full range of observed latitudes. Table 1 suggests that the higher latitude waves appear to be characterised by higher m-numbers. Given that at high latitudes the available particle populations are of low energy, and drift relatively slowly, such larger m-numbers are required in order to satisfy the drift resonance equation, Eq. (2). Unlike the lower latitude observations, at SPEAR the observed wave period is comparable to the particle bounce period at the proposed particle energies of 10 keV, thus some process involving particle bounce cannot be ruled out as a source mechanism, and conjugate spacecraft measurements will be needed to provide a completely definitive answer as to the exact generation mechanism.

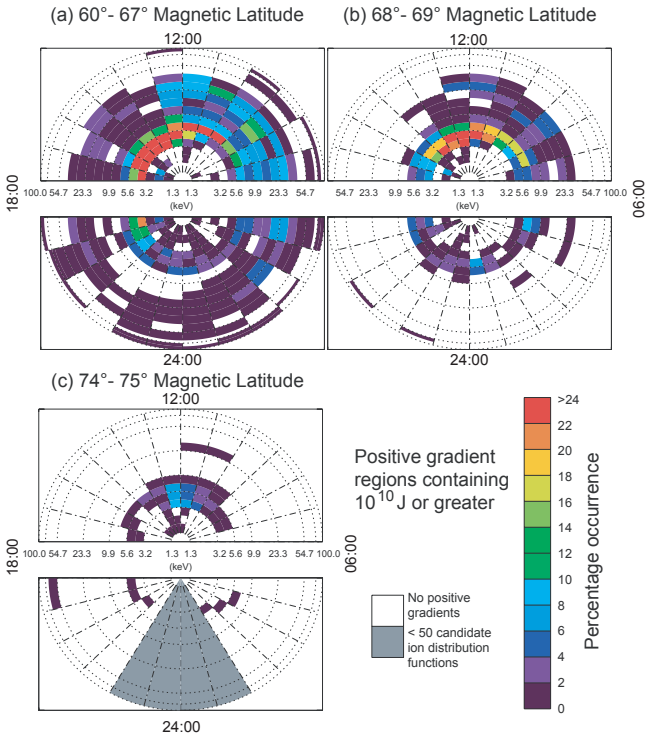

Fig. 7. The occurrence distributions of bump-on-tail ion distribution functions as a function of particle enegy and magnetic local time as observed by the Polar CAMMICE instrument for **(a)** 60°–67° N magnetic latitude **(b)** 68°–69° N magnetic latitude **(c)** 74°–75° N magnetic latitude (after Wilson et al., 2006)

5 Conclusions

Data have been presented illustrating both large-scale and small-scale ULF wave phenomena as measured by backscatter which has been artificially-induced in the Hankasalmi and Þykkvibær SuperDARN radars by the SPEAR high power HF facility on Svalbard. In the case of large-scale ULF waves, an excellent agreement is found between the ionospheric flow velocities and the ground magnetic field measurements from a nearby magnetometer, once account has been taken of the 90° rotation of the ULF wave field as it passes from the magnetosphere, through the ionosphere, to the ground. For small scale waves, the signature in the ground magnetometer data is strongly attenuated, as previous results have suggested. The artificial backscatter technique still provides clear measurements of the wave field in this case, but at the long radar ranges at which SPEAR stimulates backscatter in the Hankasalmi and Þykkvibær fields-of-view the data from each radar must be treated separately, as sufficient spatial resolution is only available along the radar beam, where 15 km range gates are employed. The spatial resolution across the beams is ∼113 km, some 8 times lower than the resolution along the beam, and this is insufficient to resolve the wave characteristics.

The radar data have revealed a high-m ULF wave event with an equatorward phase propagation of 0.4 km s^{-1} and a westward phase propagation of 0.5 km s^{-1}, equivalent to an azimuthal wave number, m, of ~ -60. This represents the first observations of ULF waves with such characteristics at the high latitudes of Svalbard. The wave event is similar to previous observations of ULF waves with equatorward and westward phase propagation at lower latitudes. The waves at all latitudes are consistent with a driving mechanism where energy in population inversions in the overlying magnetospheric energetic particles is fed into the ULF wave field through a drift resonance interaction. The particle energies of these populations decreases as latitude increases, and it appears that suitable ion distribution functions exist in the overlying magnetosphere for each latitude at which wave events have been observed.

Acknowledgements. We would like to thank the staff of the EISCAT Scientific association for their help in running SPEAR experiments.

Topical Editor K. Kauristie thanks M. Rietveld and another anonymous referee for their help in evaluating this paper.

References

Allan, W., Poulter, E. M., and Nielsen, E.: STARE observations of a Pc5 pulsation with large azimuthal wave number, J. Geophys. Res., 87, 6163–6172, 1982.

Allan, W., Poulter, E. M., and Nielsen, E.: Pc5 pulsations associated with ring current proton drifts: STARE radar observations, Planet. Space Sci., 31, 1279–1289, 1983.

Anderson, B. J., Engebretson, M. J., Rounds, S. P., Zanetti, L. J., and Potemra, T. A.: A statistical study of Pc 3-5 pulsations observed by the AMPTE/CCE magnetic fields experiment. 1. Occurrence distributions, J. Geophys. Res., 95, 10 495–10 523, 1990.

Baddeley, L. J., Yeoman, T. K., Wright, D. M., Trattner, K. J., and Kellet, B. J.: Statistical study of unstable particle populations in the global ring current and their relation to the generation of high m ULF waves, Ann. Geophys., 22, 4229–4241, 2004, http://www.ann-geophys.net/22/4229/2004/.

Baddeley, L. J., Yeoman, T. K., and Wright, D. M.: HF Doppler sounder measurements of the ionospheric signatures of small scale ULF waves, Ann. Geophys., 23, 1807–1820, 2005a, http://www.ann-geophys.net/23/1807/2005/.

Baddeley, L. J., Yeoman, T. K., Wright, D. M., Trattner, K. J., and Kellet, B. J.: On the coupling between unstable magnetospheric particle populations and resonant high m ULF wave signatures in the ionosphere, Ann. Geophys., 23, 567–577, 2005b, http://www.ann-geophys.net/23/567/2005/.

Chisham, G. and Orr, D.: Statistical studies of giant pulsations (Pgs): harmonic mode, Planet. Space Sci., 39, 999–1006, 1991.

Chisham, G., Lester, M., Milan, S. E., Freeman, M. P., Bristow, W. A., Grocott, A., McWilliams, K. A., Ruohoniemi, J. M., Yeoman, T. K., Dyson, P. L., Greenwald, R. A., Kikuchi, T., Pinnock, M., Rash, J. P. S., Sato, N., Sofko, G. J., Villain, J.-P., and Walker, A. D. M.: A decade of the Super Dual Auroral Radar Network (SuperDARN): scientific achievements, new techniques and future directions, Surv. Geophys., 28, 33–109, 2007.

Cowley, S. W. H. and Ashour-Abdallah, M.: Adiabatic plasma convection in a dipole field: Proton forbidden-zone effects for a simple electric field model, Planet. Space Sci., 24, 821–833, 1976.

Engebretson, M. J., Murr, D. L., Erickson, K. N., Strangeway, R. J., Klumpar, D. M., Fuselier, S. A., Zanetti, L. J., and Potemra, T. A.: The spatial extent of radial magnetic pulsation events observed in the dayside near synchronous orbit, J. Geophys. Res., 97, 13 741–13 758, 1992.

Grant, I. F., McDiarmid, D. R., and McNamara, A. G.: A class of high-m pulsations and its auroral radar signature, J. Geophys. Res., 97, 8439–8451, 1992.

Greenwald, R. A., Weiss, W., Nielsen, E., and Thomson, N. P.: STARE: A new radar auroral backscatter experiment in northern Scandinavia, Radio Sci., 13, 1021–1039, 1978.

Greenwald, R. A., Baker, K. B., Dudeney, J. R., Pinnock, M., Jones, T. B., Thomas, E. C., Villain, J.-P., Cerisier, J.-C., Senior, C., Hanuise, C., Hunsucker, R. D., Sofko, G., Koehler, J., Nielsen, E., Pellinen, R., Walker, A. D. M., Sato, N., and Yamagishi, H.: DARN/SUPERDARN A global view of the dynamics of high-latitude convection, Space Sci. Rev., 71, 761–796, 1995.

Hughes, W. J.: Hydromagnetic waves in the magnetosphere, in: Solar Terrestrial Physics, edited by: Carovillano, R. L. and Forbes, J. M., Reidel, Dordrecht, 1983.

Hughes, W. J. and Southwood, D. J.: The screening of micropulsation signals by the atmosphere and ionosphere, J. Geophys. Res., 81, 3234–3240, 1976.

Hughes, W. J., McPherron, R. L., Barfield, J. N., and Mauk, B. H.: A compressional Pc4 pulsation observed by three satellites in geostationary orbit near local midnight, Planet. Space Sci., 27, 821–840, 1979.

Kokubun, S.: Statistical characteristics of Pc5 waves at geostationary orbit, J. Geomag. Geoelectr., 37, 759–779, 1985.

Lessard, M. R., Hudson, M. K., and Lühr, H.: A statistical study of Pc 3-Pc 5 magnetic pulsations observed by the AMPTE/Ion Release Module satellite, J. Geophys. Res., 104, 4523–4538, 1999.

Lühr, H.: The IMAGE magnetometer network, STEP International Newsletter, 4, 4–6, 1994.

McNamara, A. G., McDiarmid, D. R., Sofko, G. J., Koeler, J. A., Forsyth, P. A., and Moorcroft, D. R.: BARS – a dual bistatic auroral radar system for the study of electric fields in the Canadian sector of the auroral zone, Adv. Space Res., 2, 145–148, 1983.

Nielsen, E., Guttler, W., Thomas, E. C., Stewart, C. P., Jones, T. B., and Hedburg, A.: SABRE – new radar-auroral backscatter experiment, Nature, 304, 712–714, 1983.

Ozeke, L. G. and Mann, I. R.: Modeling the properties of high *m* Alfvén waves driven by the drift-bounce resonance mechanism, J. Geophys. Res., 106, 15 583–15 597, 2001.

Rietveld, M. T., Kohl, H., Kopka, H., and Stubbe, P.: Introduction to ionospheric heating at Tromsø – I. Experimental overview, J. Atmos. Terr. Phys., 55, 577–599, 1993.

Robinson, T. R., Yeoman, T. K., Dhillon, R. S., Lester, M., Thomas, E. C., Thornhill, J. D., Wright, D. M., van Eyken, A. P., and McCrea, I. W.: First observations of SPEAR induced artificial backscatter from CUTLASS and the EISCAT Svalbard radars, Ann. Geophys., 24, 291–309, 2006, http://www.ann-geophys.net/24/291/2006/.

Southwood, D. J.: A general approach to low-frequency instability in the ring current plasma, J. Geophys. Res., 81, 3340–3348, 1976.

Southwood, D. J., Dungey, J. W., and Etherington, R. J.: Bounce resonant interactions between pulsations and trapped particles, Planet. Space Sci., 17, 349–361, 1969.

Takahashi, K., Higbie, P. R., and Baker, D. N.: Azimuthal propagation and frequency characteristic of compressional Pc5 waves observed at geostationary orbit, J. Geophys. Res., 90, 1473–1485, 1985.

Takahashi, K., McEntire, R. W., Lui, A. T. Y., and Potemra, T. A.: Ion flux oscillations associated with a radially polarised transverse Pc5 magnetic pulsation, J. Geophys. Res., 95, 3717–3731, 1990.

Takahashi, K., Sato, N., Warnecke, J., Lühr, H., Spence, H. E., and Tonegawa, Y.: On the standing wave mode of giant pulsations, J. Geophys. Res., 97, 10 717–10 732, 1992.

Tian, M., Yeoman, T. K., Lester, M., and Jones, T. B.: Statistics of Pc5 pulsation events observed by SABRE, Planet. Space Sci., 39, 1239–1247, 1991.

Waldock, J. A., Jones, T. B., and Southwood, D. J.: First results of micropulsation activity observed by SABRE, Planet. Space Sci., 31, 573–578, 1983.

Wilson, M. E., Yeoman, T. K., Baddeley, L. J., and Kellet, B. J.: A Statistical Investigation of the Invariant Latitude Dependence of Unstable Magnetospheric Ion Populations in Relation to High *m* ULF Wave Generation, Ann. Geophys., 24, 3027–3040, 2006, http://www.ann-geophys.net/24/3027/2006/.

Woch, J., Kremser, G., and Korth, A.: A comprehensive investigation of compressional ULF waves observed in the ring current, J. Geophys. Res., 95, 15 113–15 132, 1990.

Wright, D. M., Yeoman, T. K., and Chapman, P. J.: High-latitude HF Doppler observations of ULF waves: 1. waves with large spatial scale sizes, Ann. Geophys., 15, 1548–1556, 1997, http://www.ann-geophys.net/15/1548/1997/.

Wright, D. M., Davies, J. A., Robinson, T. R., Chapman, P. J., Yeoman, T. K., Thomas, E. C., Lester, M., Cowley, S. W. H., Stocker, A. J., Horne, R. B., and Honary, F.: Space Plasma Exploration by Active Radar (SPEAR): an overview of a future radar facility, Ann. Geophys., 18, 1248–1255, 2000, http://www.ann-geophys.net/18/1248/2000/.

Yeoman, T. K. and Wright, D. M.: ULF waves with drift resonance and drift-bounce resonance energy sources as observed in artificially-induced HF radar backscatter, Ann. Geophys., 19, 159–170, 2001, http://www.ann-geophys.net/19/159/2001/.

Yeoman, T. K., Tian, M., Lester, M., and Jones, T. B.: A study of Pc5 hydromagnetic waves with equatorward phase propagation, Planet. Space Sci., 40, 797–810, 1992.

Yeoman, T. K., Wright, D. M., Chapman, P. J., and Stockton-Chalk, A. B.: High-latitude observations of ULF waves with large azimuthal wavenumbers, J. Geophys. Res., 105, 5453–5462, 2000.

Yeoman, T. K., Wright, D. M., Stocker, A. J., and Jones, T. B.: An evaluation of range accuracy in the SuperDARN over-the-horizon HF radar systems, Radio Sci., 36, 801–813, 2001.

Yeoman, T. K., Wright, D. M., and Baddeley, L. J.: Ionospheric Signatures of ULF Waves: Active Radar Techniques, in: Magnetospheric ULF Waves: Synthesis and New Directions, edited by Takahashi, K., Chi, P. J., Denton, R. E., and Lysak, R. L., American Geophysical Union, 2006.